

Chapter 14

Millimeter-Wave Pattern Reconfigurable Antenna

Muhammad Kamran Saleem and Majeed A.S. Alkanhal

14.1 Introduction

Antennas are considered to be one of the most essential and significant elements of any wireless communication system. The commonly used antennas in a wireless communications system are monopoles, dipoles, loop antenna, horn antenna, and microstrip antenna. Each type of antenna possesses its own advantages and disadvantages that make it suitable for particular application. The initial design properties of these antennas such as bandwidth, frequency of operation, radiation characteristics, etc. are fixed and cannot be changed. The modern transmitting and receiving systems demand increased functionality such as direction finding, radars, beam steering, and command and control within a confined area. The reconfigurable antennas are a solution to tackle these challenges. The reconfigurability in an antenna is achieved by intentionally changing its frequency of operation, polarization, or radiation characteristics. This change is accomplished by various techniques that reallocate the antenna currents and thus changes electromagnetic fields of the antenna's effective aperture. Figure 14.1 describes the reconfiguration techniques that are mostly based on the integration of switches such as radio frequency microelectromechanical systems (RF-MEMS), PIN diodes, varactors, and photoconductive elements. Furthermore, the application of smart materials such as ferrites and liquid crystals can also be utilized for physical alteration of the antenna radiating structure, to achieve required reconfigurability in antenna operation.

M.K. Saleem (✉)

Electrical Engineering Department, University of Central Punjab, Lahore, Pakistan
e-mail: mksa05@gmail.com

M.A.S. Alkanhal

Electrical Engineering Department, King Saud University, Riyadh, Saudi Arabia

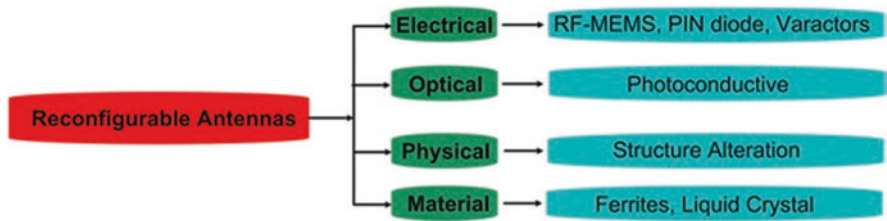


Fig. 14.1 Techniques adopted to achieve reconfigurable antennas

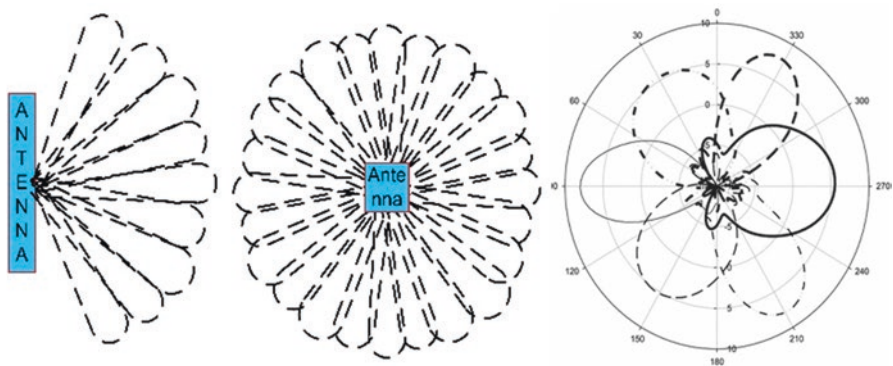


Fig. 14.2 Antenna with reconfigurable radiation patterns

The term reconfigurable antenna is broad and extends to antennas that can change their parameters such as impedance bandwidth, frequency of operation, polarization, and radiation pattern [1–3]. In this chapter the focus will be on the class of reconfigurable antennas with the capability of altering their radiation patterns in the far field; the presented work is an extension to research work published previously in [4]. This reconfiguration of antenna radiation pattern can be utilized efficiently for power/energy by directing signals only toward the intended directions, avoiding noisy sources, improving system gain and security, etc. The antenna radiation pattern reconfigurability is illustrated in Fig. 14.2, where a single element antenna or an antenna array can have more than one radiation patterns associated with it. The design and development of these radiation pattern reconfigurable antennas poses many challenges, not only in obtaining the desired levels of antenna functionality but also in the implementation of the antenna itself. However, in most of the ILAs the degradation of gain, beamwidth, and side lobe level of antenna radiation beams particularly due to interelement coupling and shadow effect at the two extreme edges of scanning range is inevitable [5–8].

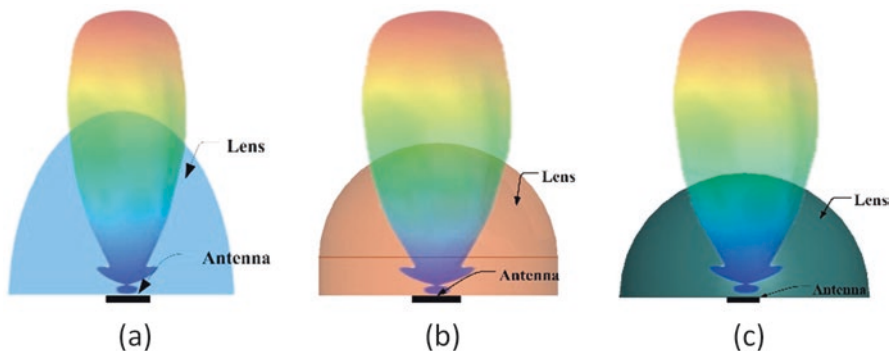


Fig. 14.3 Dielectric lenses. (a) Hemispherical lens, (b) extended hemispherical lens, (c) elliptical lens

14.2 Dielectric Lens for Millimeter-Wave Applications

The commonly used dielectric lenses are found in shape of hemispherical or extended hemispherical [3], elliptical, or cylindrical as shown in Fig. 14.3. The dielectric lenses can be made up of various materials with low or high dielectric permittivity such as Teflon and Rexolite. The hemispherical, extended hemispherical, and elliptical lenses are usually utilized to enhance antenna gain in broadside direction and are very promising candidates for millimeter-wave antennas with beam steering applications. The extended hemispherical lens as shown in Fig. 14.3b is preferred over elliptical and hemispherical lenses since it is easy to manufacture. Furthermore, the antenna feed is placed at the bottom of the lens, providing a broadside radiation pattern.

14.3 Microstrip Patch Antenna for 60 GHz Applications

The configuration of a simple microstrip patch antenna (MPA) is shown in Fig. 14.4. The MPA is placed over Rogers RT/duroid 5880 substrate ($\epsilon_r = 2.2$) having thickness of 0.254 mm. The bottom side of substrate is fully copper plated ($th = 0.018$ mm) and acts as antenna ground plane. The important design parameters of MPA are shown in Fig. 14.4b. The initial dimensions for MPA are calculated by conventional set of equations given in [9]. The MPA structure having a tapered feed is optimized, utilizing the 3D EM solver ANSYS HFSS [10] to achieve required bandwidth and gain. The optimum dimensions are found to be: $T_1 = T_2 = T_3 = 1.07$ mm, $L_m = 11.96$ mm, $L_1 = 0.5$ mm, $L_p = 1.56$ mm, $W_p = 2.08$ mm, $L = 21.73$ mm, $W = 13$ mm.

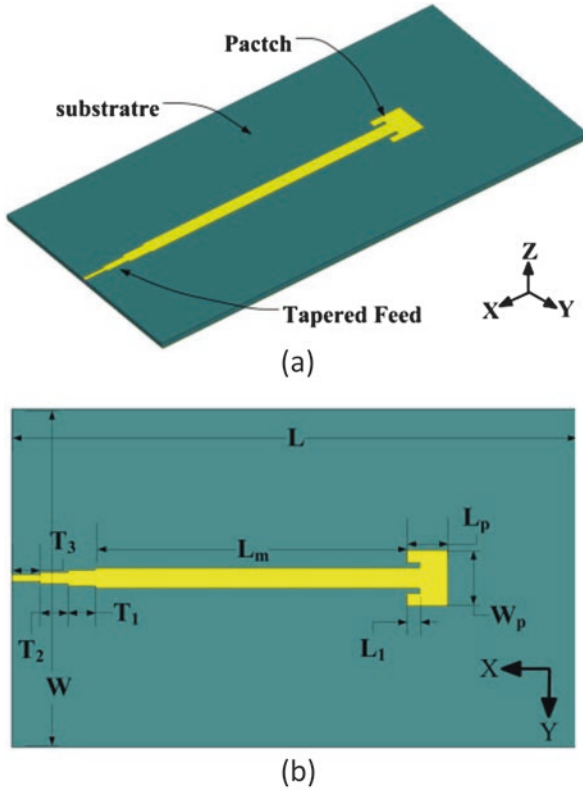


Fig. 14.4 MPA structure for 60 GHz applications. (a) 3D configuration, (b) top view

The structure of MPA is optimized and the impedance bandwidth is found to be 4.5 GHz (58–62.5 GHz) as shown in Fig. 14.5. The antenna 3 dB beamwidth for the two radiation patterns in two orthogonal plans, i.e., in YZ -plane and XZ -plane, is found to be 64° and 102° , respectively, as shown in the 2D normalized radiation pattern in Fig. 14.6. The realized gain is found to be above 6 dB in most of the frequency band of operation as shown in Fig. 14.7. It can also be observed that the maximum gain is found to be 7.5 dB at 61.5 GHz.

14.3.1 Dielectric Lens Integration with MPA

The integration of an extended hemispherical (Teflon) have ϵ_r of 2.1 lens is made to the MPA structure presented previously. The structure of MPA with extended hemispherical Teflon lens is shown in Fig. 14.8. The alignment markers are utilized to place the dielectric lens at specified location.

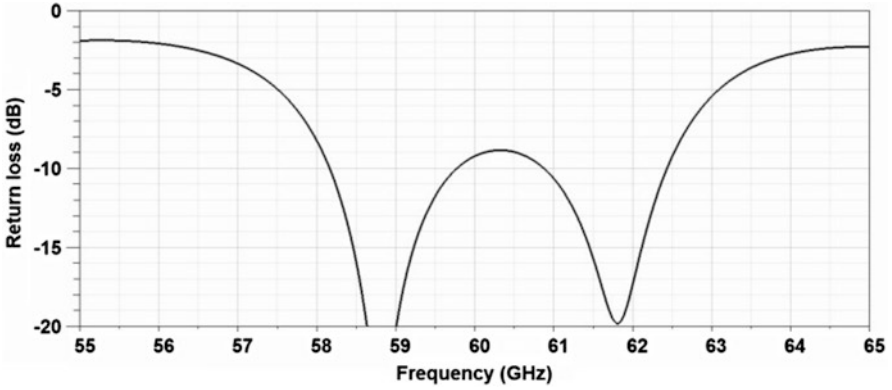


Fig. 14.5 Simulated return loss of MPA

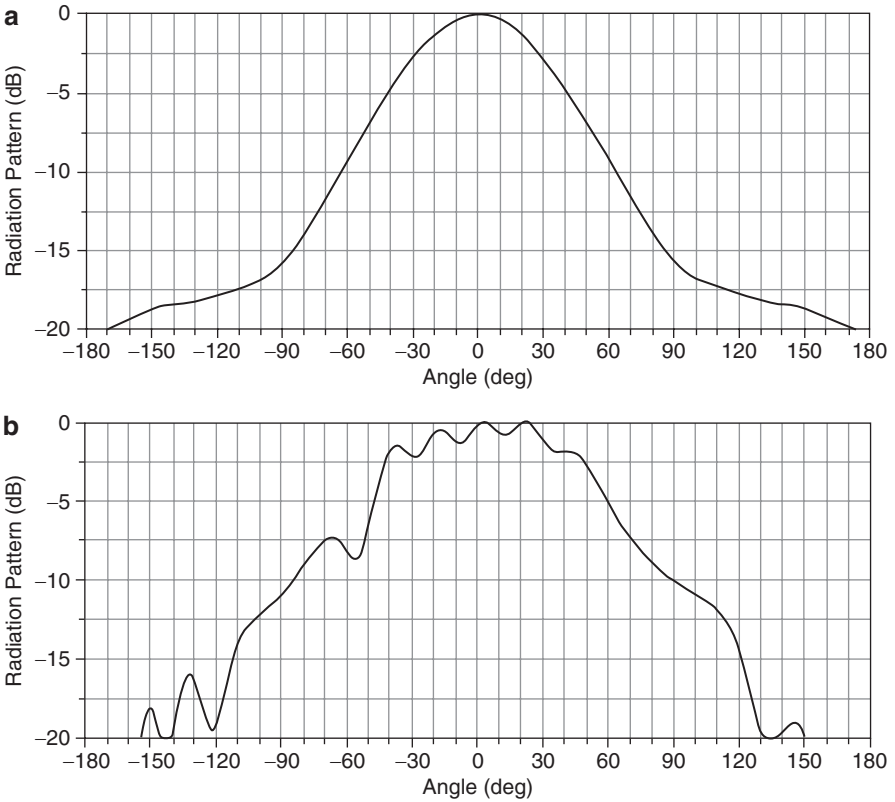


Fig. 14.6 MPA simulated radiation patterns. (a) YZ-plane, (b) XZ-plane

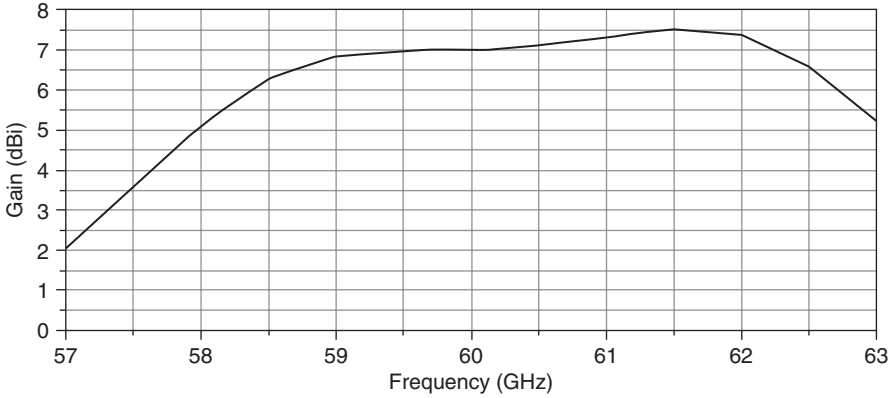
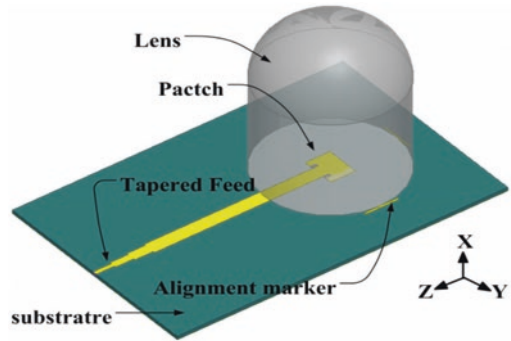


Fig. 14.7 MPA simulated gain

Fig. 14.8 Structure of MPA with extended hemispherical Teflon lens



The extended hemispherical lens is placed over the MPA. The side and top view of MPA structure integrated with extended hemispherical dielectric lens is shown in Fig. 14.9. The extended hemispherical dielectric lens consists of a Teflon cylinder ($\epsilon_r = 2.1$) with a Teflon half sphere on top. The height and diameter of the cylinder are referred to as H and D , respectively, whereas the radius of the top half sphere is referred to as R . The procedure given in [11] is employed to design the extended hemispherical lens. The initial radius of top hemispherical part was chosen to be λ_g (where λ_g is guided wavelength in Teflon), resulting in cylindrical extension height $H_1 = 8.8$ mm. The center of MPA and center of lens are aligned. A tedious optimization is carried out over the structure of the MPA with extended hemispherical lens to achieve maximum impedance bandwidth, gain, and radiation beamwidth of 24° . The inset of MPA (g) is optimized keeping in mind the available manufacturing tolerances. However, a special attention is given to widths of tapered feed (W_3) so that a V-band connector can easily be connected to the feed point. The optimum dimensions for the MPA with extended hemispherical lens are found to be: $D = 8$ mm, $H_1 = 7$ mm, $H_2 = R = 4$ mm, $T_1 = T_2 = T_3 = 1.1$ mm, $W_1 = 0.62$ mm,

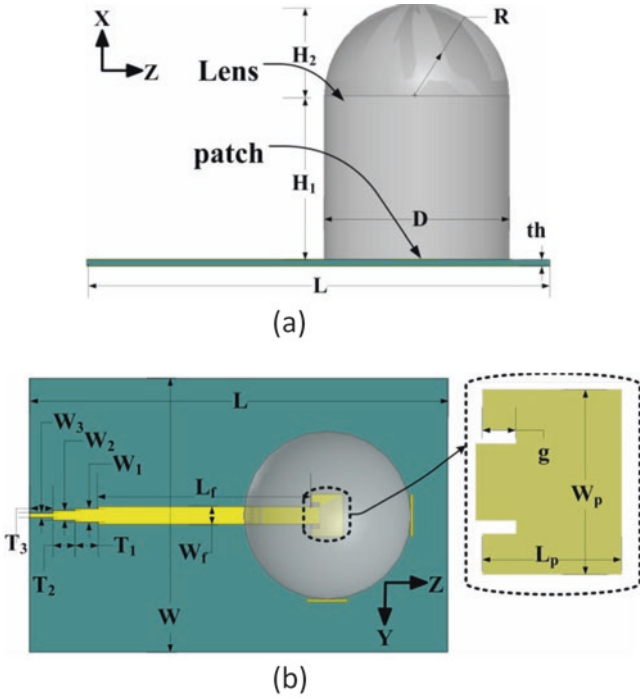


Fig. 14.9 Structure of MPA with Teflon lens with important design parameters. (a) Side view, (b) top view

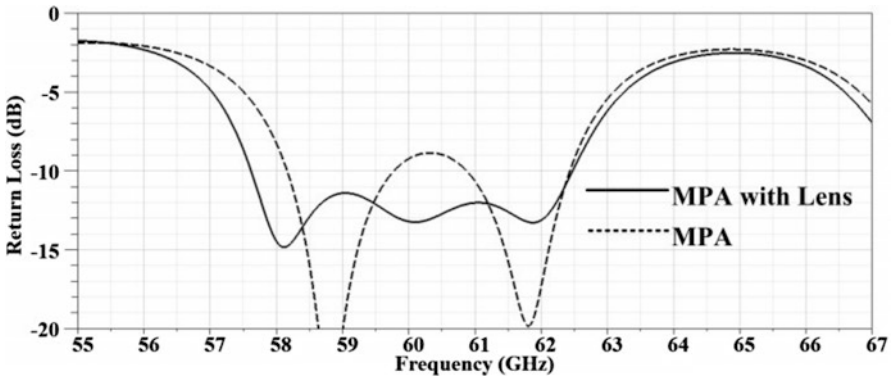


Fig. 14.10 Comparison between simulated return loss of MPA and MPA integrated with dielectric lens

$W_2 = 0.43$ mm, $W_3 = 0.23$ mm, $L_f = 10.2$ mm, $W_f = 0.824$ mm, $g = 0.35$ mm, $L_p = 1.5$ mm, $W_p = 2.02$ mm, $L = 20$ mm, $W = 13$ mm.

The simulated return loss of the optimized MPA and MPA with dielectric lens is compared in Fig. 14.10. The simulated return loss bandwidth of both antennas,

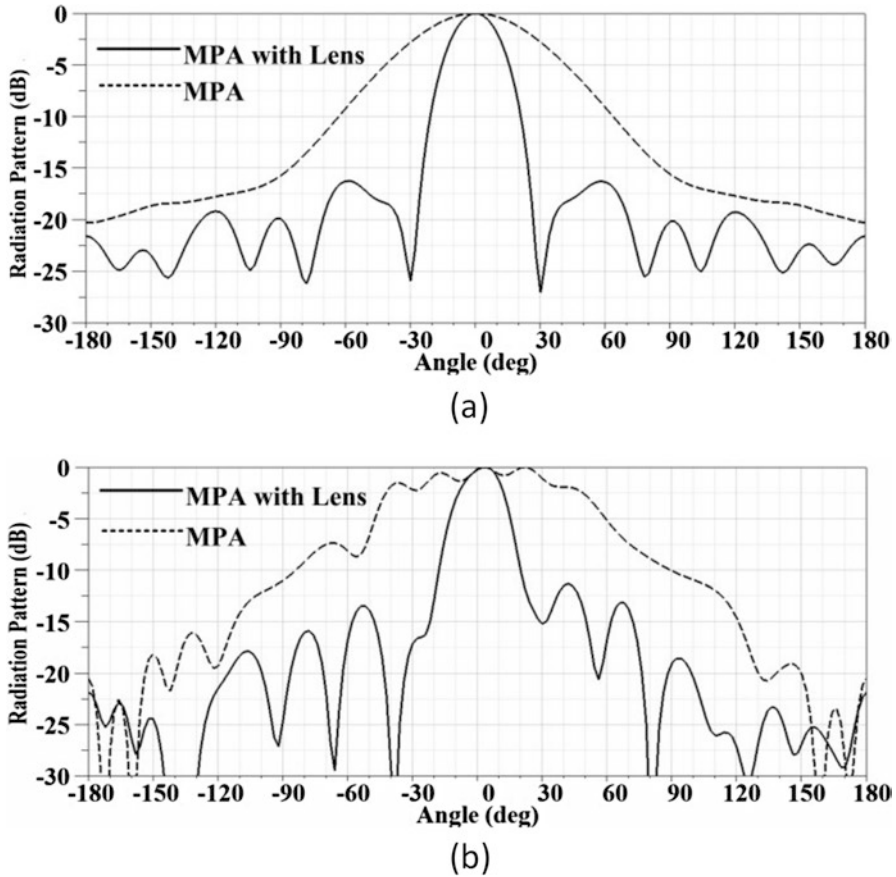


Fig. 14.11 Simulated normalized radiation pattern of MPA and MPA integrated with lens. (a) XZ-plane, (b) XY-plane

i.e., MPA and MPA with dielectric lens, is found to be approximately 5 GHz (57.5–62.5 GHz).

In Fig. 14.11 the comparison between the simulated radiation pattern of MPA and MPA with extended hemispherical dielectric lens in two orthogonal planes at 60 GHz is shown. As illustrated in Fig. 14.11a the 3 dB beamwidth in XZ-plane is found to be 64° and 24° for MPA and MPA with lens, respectively, whereas in Fig. 14.11b the 3 dB beamwidth in XY-plane is found to be 102° and 24° for MPA and MPA with lens, respectively. It is important to mention that the side lobe level in case of MPA with lens is below 16 dB and 12 dB in both XZ-plane and XY-plane. For a better understanding of radiation pattern characteristics the 3D radiation patterns of MPA and MPA with lens are shown in Fig. 14.12. It can be easily observed that when utilizing an extended hemispherical dielectric lens, the radiation pattern of the simple MPA is varied and a uniform beamwidth in both orthogonal planes is achieved. As seen in Fig. 14.12b the 3 dB beamwidth in XZ-plane and XY-plane is found to be very similar, i.e., approximately 24° as shown in Fig. 14.11. This gives

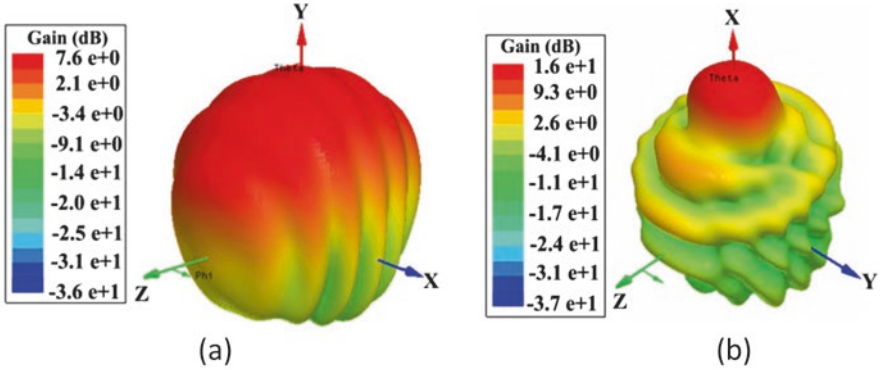


Fig. 14.12 3D radiation patterns. (a) MPA, (b) MPA integrated with lens

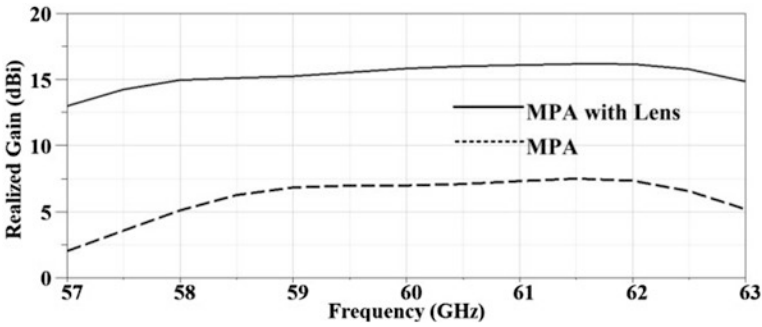


Fig. 14.13 Simulated realized gain of MPA and MPA integrated with lens

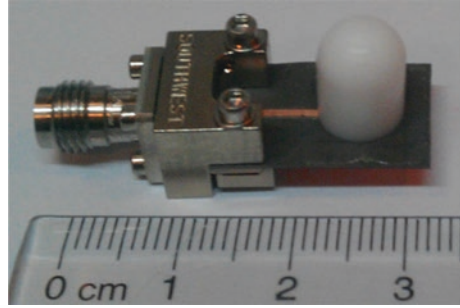
the proposed antenna structure an added advantage especially for applications involving the beam switching techniques.

Furthermore, as expected the gain of conventional MPA is enhanced by 9 dB by integration of the extended hemispherical dielectric lens as shown in Fig. 14.13. The maximum gain of MPA with lens is found to be 16.25 dBi at 61.5 GHz, whereas it remains above 15 dBi in most of the frequency bands of operation, i.e., from 58.5 to 62.5 GHz.

A prototype is fabricated to verify the simulation results of MPA integrated with extended hemispherical dielectric lens. The photograph of the fabricated prototype of MPA integrated with Teflon lens and V-band connector is shown in Fig. 14.14. The MPA was manufactured utilizing the LPKF (Laser). However, the dielectric lens (Teflon) is glued over the MPA utilizing a very thin layer of 3 M glue film (50 μm). Furthermore, the V-band removable connector is connected to the tapered feed for test and measurement purpose.

The comparisons between the simulated and measured results of MPA with extended hemispherical dielectric lens are shown in Fig. 14.15, which are found to be in good agreement. The return loss measurement of developed prototype is

Fig. 14.14 Fabricated MPA with extended hemispherical dielectric lens, MPA and V-band connector



performed by utilizing Anritsu vector network analyzer. The impedance bandwidth of 5 GHz (57.5–62.5 GHz) is achieved as shown in Fig. 14.15a. The antenna radiation pattern is obtained by utilizing a custom base system consisting of V-band horn, VNA, V-band cables and contactors, and AUT (antenna under test). As shown in Fig. 14.15b, c, the 3 dB beamwidth is found to be 24° in both XZ -plane and XY -plane, whereas the side lobe level is found to be below 16 dB and 12 dB in both XZ -plane and XY -plane, respectively, at 60 GHz. The small variation observed between the simulated and measured results is probably due to 3 M glue film ($50\ \mu\text{m}$) used to fix the lens and the presence of V-band connector.

14.3.2 Element MPA Array with Extended Hemispherical Teflon Lenses

In this section the simulation and measured results of 15-element microstrip patch antenna (MPA) array with hemispherical dielectric (Teflon) lenses operating in 60 GHz band are presented. The MPA with extended hemispherical dielectric lens described in previous section is utilized to form a circular array as shown in Fig. 14.16. The dimensions of dielectric lens (Teflon) and MPA are kept the same as mentioned before. The array is designed to cover a wide scan angle of full 360° in azimuth plane ($\theta = 90^\circ$) with impedance bandwidth of 5 GHz (57.5–62.5 GHz) and gain higher than 16 dB and 3 dB crossover. The array support is made of acrylonitrile butadiene styrene (ABS), since it is a low-cost plastic, easy to machine, ideal material for structural applications, and easy to glue with other materials. The ABS support is necessary part for the antenna development and measurements since all single element MPAs with Teflon lens are glued over this support to develop a prototype for test and measurements. The dielectric constant of ABS material varies in range of 2–3.5. The simulations are carried out with various different dielectric constants and no abnormality in results is observed.

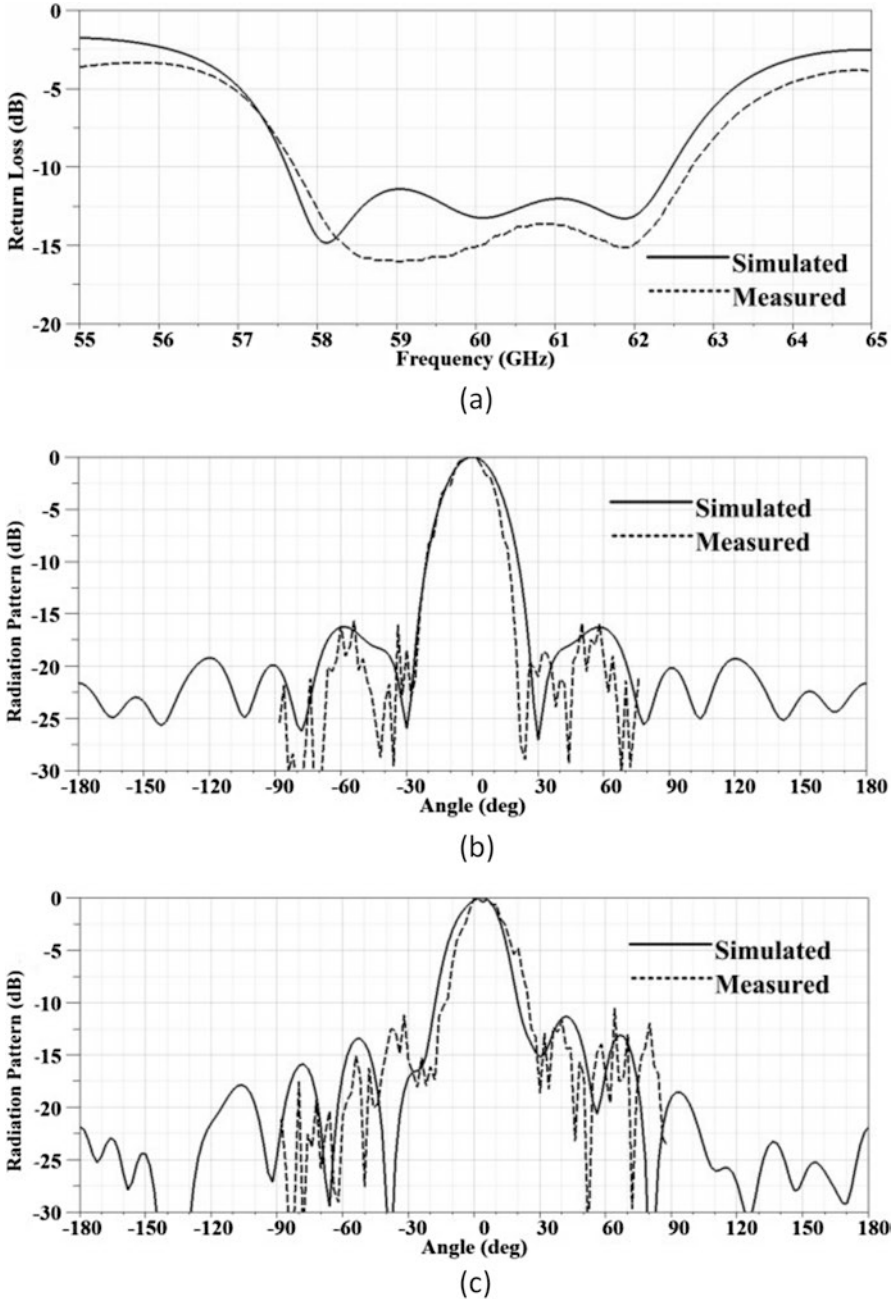


Fig. 14.15 Comparison between simulated and measured results of MPA with lens. (a) Return loss, (b) XZ-plane normalized radiation pattern at 60 GHz, (c) XY-plane normalized radiation pattern at 60 GHz

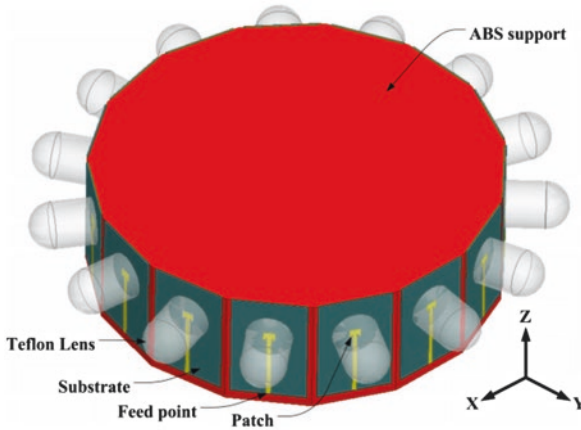


Fig. 14.16 15-element circular microstrip patch antenna array with dielectric lenses (3D view)

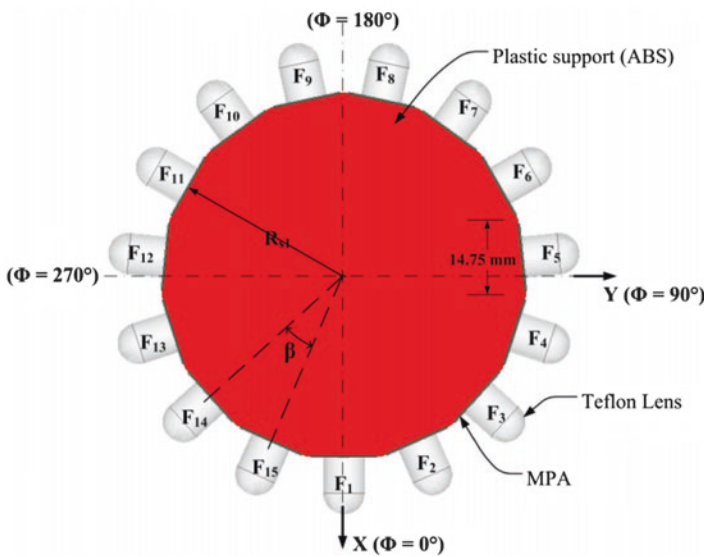


Fig. 14.17 15-element circular patch antenna array with integrated lenses (top view)

The top view of the 15-element circular array is shown in Fig. 14.17. As shown the ABS support consists of 15 edges each having length of 14.75 mm. The angular distance between the adjacent elements is set to be $\beta = 24^\circ$ to achieve full 360° coverage in azimuthal plane and 3 dB crossover. By activating each array element one by one while all others are terminated by 50Ω termination, the antenna beam is scanned over the whole 360° in azimuth plane with 3 dB crossover. Some important

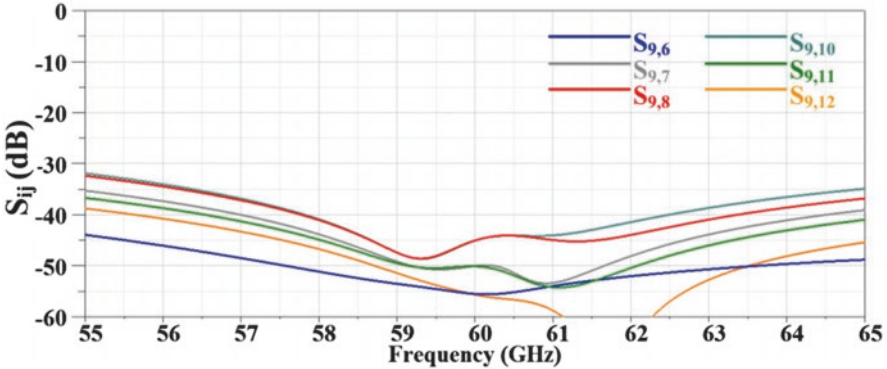


Fig. 14.18 Mutual coupling between array elements

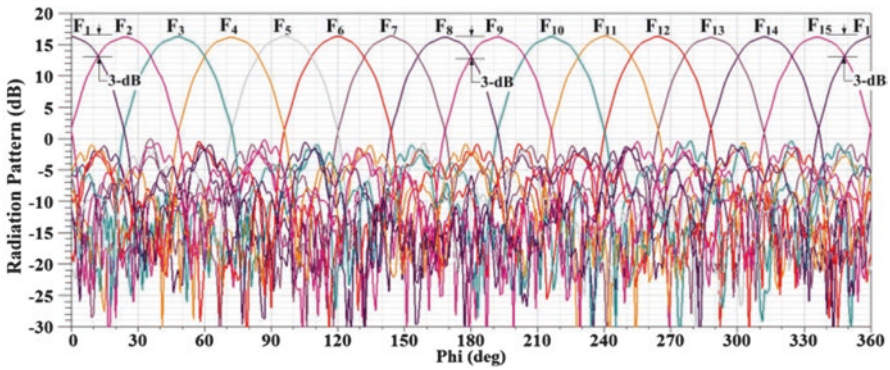


Fig. 14.19 Simulated 2D radiation pattern in azimuth plane ($\theta = 90^\circ$) of 15-element circular patch antenna array with integrated lenses (zoomed)

array parameters as mentioned in Fig. 14.17 are $R_a = 35.01$ mm, $S = 14.55$ mm, and $\beta = 24^\circ$, where R_a and β are optimized to achieve 3 dB crossover between the neighboring radiation patterns.

The mutual coupling between the array elements is one of the important parameters, especially in antennas with reconfigurable radiation patterns. With the proposed antenna array structure the mutual coupling between the array elements is found to be below -35 dB in required frequency band of operation as shown in Fig. 14.18.

The 2D radiation pattern in azimuth plane ($\theta = 90^\circ$) of the 15-element MPA array with Teflon lenses is shown in Fig. 14.19. The simulations are carried out by exciting each feed (MPA integrated with Teflon lens) one by one while all other feeds are terminated by a matched load. The 3 dB crossover between the adjacent MPA feeds is achieved. The 3 dB beamwidth is found to be approximately 24° having side lobe level below -18 dB, and constant gain is achieved in whole scan range for radiation pattern from each feed (i.e., $F_1, F_2, F_3, \dots, F_{15}$).

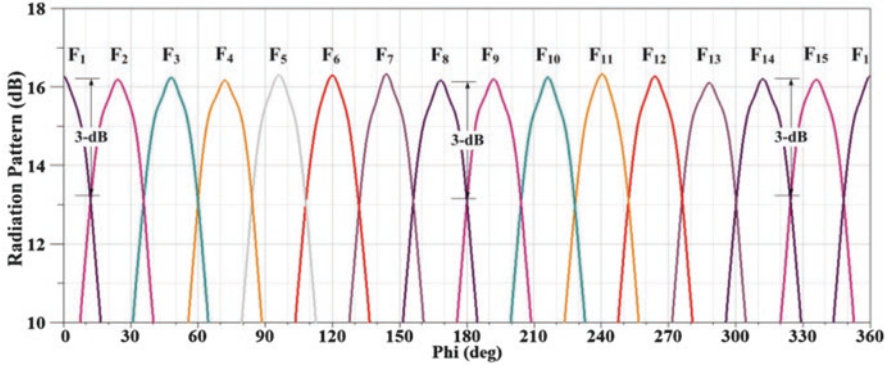


Fig. 14.20 Simulated 2D radiation pattern in azimuth plane ($\theta = 90^\circ$) of 15-element circular patch antenna array with integrated lenses (zoomed)

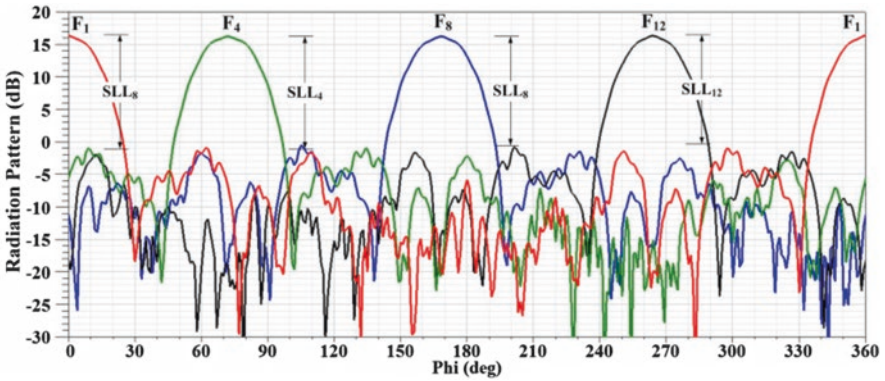


Fig. 14.21 Simulated 2D radiation pattern in azimuth plane ($\theta = 90^\circ$) from 15-element circular patch antenna array with integrated lenses (radiation patterns from feed 1, feed 4, feed 8, and feed 12 are shown for clarity)

The 2D radiation pattern in azimuth plane ($\theta = 90^\circ$) of the 15-element MPA array integrated with Teflon lenses is zoomed and shown in Fig. 14.20. The antenna array covers full 360° in azimuth plane. The gain in azimuth is found to be above 16 dB for each feed. It is clearly evident that the array covers the scan range of, i.e., $\phi = 0^\circ - 360^\circ$ with 3 dB crossover.

For a better understanding of the side lobe level (SLL), the 2D radiation patterns in azimuth plane ($\theta = 90^\circ$) from the four feeds, i.e., F_1 , F_4 , F_8 , and F_{12} , are shown in Fig. 14.21. It is clearly evident that the side lobe level is almost similar for all beams $SLL_1 = SLL_4 = SLL_8 = SLL_{12} = -17$ dB. Similarly, the beamwidth of all beams generated by activating each array element one by one while all others are termi-

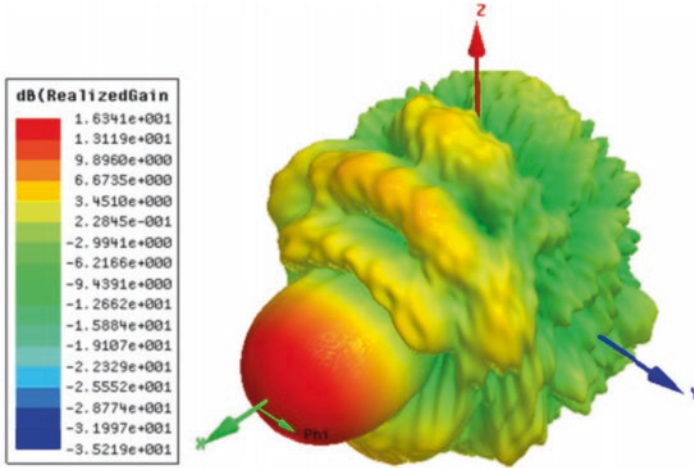


Fig. 14.22 Simulated 3D radiation pattern from 15-element circular patch antenna array with integrated lenses (feed 1 is active)

nated with 50Ω load are found to be 24° . The 3D radiation pattern achieved by activating a single array element is shown in Fig. 14.22 for a better understanding of antenna radiation properties.

The 2D radiation pattern in elevation plane ($\phi = \text{constant}$) of MPA feed 1, feed 7, and feed 13 is shown in Fig. 14.23. The 3 dB beamwidth is approximately 22.5° for all feeds with SLL of approximately 12 dB. As a conclusion the antenna is suitable for wide scan angle of $\pm 180^\circ$ (i.e., from $\phi = 0^\circ - 360^\circ$) with a gain better than 16 dB and 3 dB crossover.

To validate the proposed design, a 5-element array is developed as shown in Fig. 14.24. The five elements are referred to as F_7 , F_8 , F_9 , F_{10} , and F_{11} . The comparison between the simulated and measured return loss is shown in Fig. 14.25, which is found to be in good agreement. However, the variation between the simulated and measured results can be attributed to manual work such as placing the Teflon lens on the patch antenna, placing and connecting the removable V-band connector to the antenna printed circuit board (PCB), and gluing of array elements on ABS support.

The comparison between simulated and measured radiation pattern at 60 GHz in azimuth plane for the five elements is shown in Fig. 14.26, which are found to be in good agreement. It can be easily seen that the crossover between the adjacent array elements is at approximately 3 dB, and maximum side lobe level is found to be approximately 15 dB. The beamwidth, gain, and side lobe level of each of the beams from the array remain constant throughout the whole scan range. This gives the proposed design an advantage over the beam scanning ILAs found in literature.

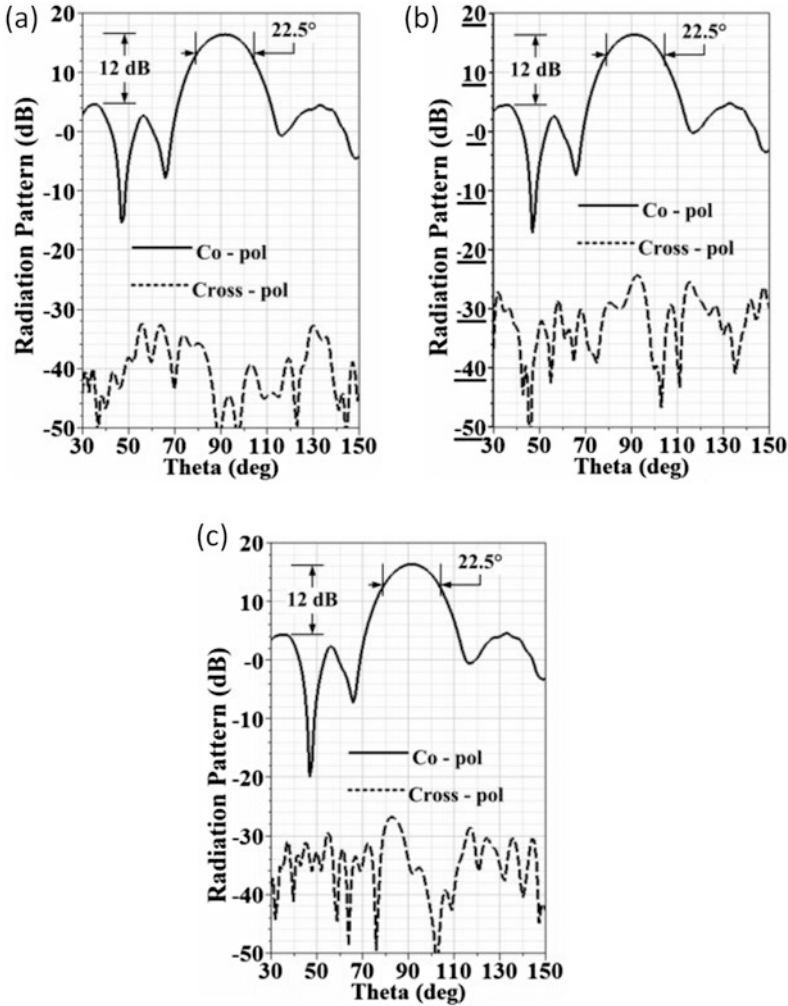


Fig. 14.23 2D radiation pattern in elevation plane ($\phi = \text{constant}$) of 15-element circular patch antenna array with lenses. (a) Feed 1, (b) feed 7, (c) feed 13

14.4 Conclusion

A 15-element antenna array operating at 60 GHz with beam switching capability in azimuth plane is proposed. The array covers a wide impedance bandwidth of 5 GHz (57.5–62.5 GHz) with gain higher than 15 dBi in frequency band of operation. The matching and the radiation characteristics of the presented switched beam antenna array are validated by measurements performed on a 5-element corresponding array prototype. A very good agreement between the measured and simulated results is

Fig. 14.24 Developed prototype of 5-element antenna array for test and measurements

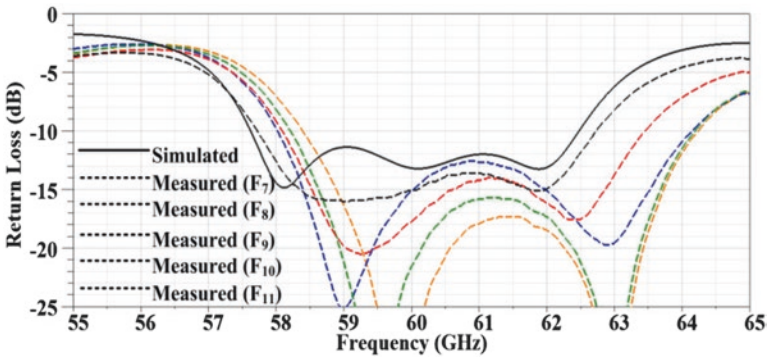
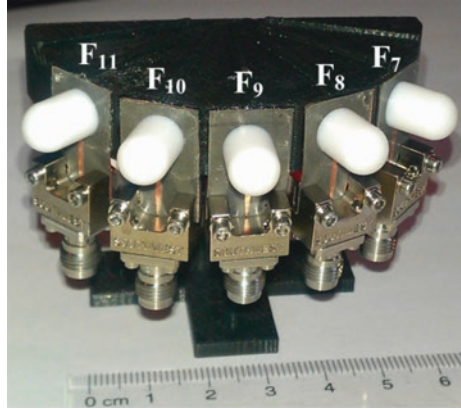


Fig. 14.25 Comparison between the simulated and measured return loss

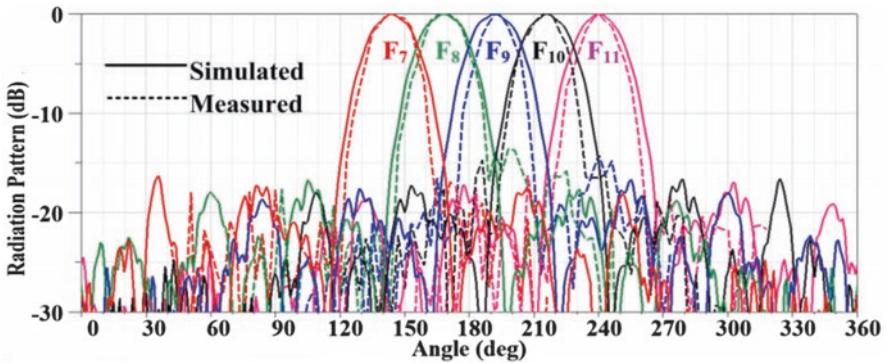


Fig. 14.26 Comparison between the simulated and measured radiation pattern

observed. The beamwidth, gain, and side lobe level of each of the beams from the array remain constant throughout the whole scan range of 360° in azimuth plane. This gives the proposed design an advantage over the beam scanning ILAs found in literature.

References

1. M.T. Jusoh, O. Lafond, F. Colombel, M. Himdi, Performance of a reconfigurable reflector antenna with scanning capability using low cost plasma elements. *Microw. Opt. Technol. Lett.* **55**, 2869–2874 (2013)
2. A. Artemenko, A. Mozharovskiy, A. Maltsev, R. Maslennikov, A. Sevastyanov, V. Sorin, Experimental characterization of e-band two-dimensional electronically beam-steerable integrated lens antennas. *IEEE Antennas Wirel. Propag. Lett.* **12**, 1188–1191 (2013)
3. B. Schoenlinner, X. Wu, J.P. Ebling, G.V. Eleftheriades, G.M. Rebeiz, Wide-scan spherical-lens antennas for automotive radars. *IEEE Trans. Microwave Theory Tech.* **50**, 2166–2175 (2002)
4. Y.J. Cheng, Y. Fan, Millimeter-wave miniaturized substrate integrated multibeam antenna. *IEEE Trans. Antennas Propag.* **59**, 4840–4844 (2011)
5. X. Ding, B.-Z. Wang, G.-Q. He, Research on a millimeter-wave phased array with wide-angle scanning performance. *IEEE Trans. Antennas Propag.* **61**, 5319–5324 (2013)
6. Y.J. Cheng, W. Hong, K. Wu, Millimeter-wave substrate integrated waveguide multibeam antenna based on the parabolic reflector principle. *IEEE Trans. Antennas Propag.* **56**, 3055–3058 (2008)
7. O. Lafond, M. Himdi, H. Merlet, P. Lebars, An active reconfigurable antenna at 60 GHz based on plate inhomogeneous lens and feeders. *IEEE Trans. Antennas Propag.* **61**, 1672–1678 (2013)
8. M. Kamran Saleem, M.A.S. Alkanhal, A. Fattah Sheta, M. Abdel Rahman, M. Himdi, Integrated lens antenna Array with full azimuth plane beam scanning capability at 60 GHz. *Microw. Opt. Technol. Lett.* **59**(1), 116–120 (2017)
9. C.A. Balanis, *Antenna Theory: Analysis and Design* (John Wiley & Sons, New York, 2012)
10. Ansys, Hfss, v14, ANSYS Corporation Software (Pittsburgh, U.S.A., 2014)
11. C.A. Fernandes, E.B. Lima, J.R. Costa, *Dielectric Lens Antennas: Handbook of Antenna Technologies*, pp 1001–1064 (Springer Singapore, 2016)